EARTHQUAKE ENGINEERING AND STRUCTURAL DYNAMICS
*Earthquake Engng Struct. Dyn.* 2007; **36**:729–749
Published online 12 December 2006 in Wiley InterScience (www.interscience.wiley.com). DOI: 10.1002/eqe.650

# Seismic control of smart base isolated buildings with new semiactive variable damper

S. Nagarajaiah[1,*,†] and S. Narasimhan[2]

[1]*Department of Civil & Environmental Engineering and Mechanical Engineering & Material Science, Rice University, Houston, TX 77005, U.S.A.*
[2]*Department of Civil and Environmental Engineering, University of Waterloo, Waterloo, Ont., Canada N2L 3G1*

SUMMARY

A new semiactive independently variable damper, SAIVD, is developed and shown to be effective in achieving response reductions in smart base isolated buildings in near fault earthquakes. The semiactive device consists of four linear visco-elastic elements, commonly known as Kelvin–Voigt elements, arranged in a rhombus configuration. The magnitude of force in the semiactive device can be adjusted smoothly in real-time by varying the angle of the visco-elastic elements of the device or the aspect ratio of the rhombus configuration. Such a device is essentially linear, simple to construct, and does not present the difficulties commonly associated with modelling and analysing nonlinear devices (e.g. friction devices). The smooth semiactive force variation eliminates the disadvantages associated with rapid switching devices. Experimental results are presented to verify the proposed analytical model of the device. A $H_\infty$ control algorithm is implemented in order to reduce the response of base isolated buildings with variable damping semiactive control systems in near fault earthquakes. The central idea of the control algorithm is to design a $H_\infty$ controller for the structural system that serves as an aid in the determination of the optimum control force in the semiactive device. The relative performance of the SAIVD device is compared to a variable friction device, recently developed by the authors in a separate study, and several key aspects of performance are discussed regarding the use of the two devices for reducing the responses of smart base isolated buildings in near fault earthquakes. Copyright © 2006 John Wiley & Sons, Ltd.

Received 10 May 2006; Revised 8 September 2006; Accepted 11 September 2006

KEY WORDS: $H_\infty$; smart base isolated buildings; variable damping; semiactive structural control

*Correspondence to: S. Nagarajaiah, Department of Civil & Environmental Engineering and Mechanical Engineering & Material Science, Rice University, Houston, TX 77005, U.S.A.
†E-mail: nagaraja@rice.edu

Contract/grant sponsor: National Science Foundation; contract/grant number: NSF-CAREER-CMS 9996290

## 1. INTRODUCTION

Semiactive systems such as variable stiffness, damping and friction devices have been investigated and demonstrated to be effective by many researchers (e.g. [1–20]). Several types of variable damping and variable friction devices have been implemented on base isolated buildings for reducing base displacements and superstructure responses (e.g. [2, 21]). Recently, Narasimhan *et al*. [22] have developed a new variable friction device, semiactive independently variable friction (SAIVF) device, and studied the effectiveness of the control strategy using a new control algorithm based on $H_\infty$ on smart base isolated buildings. The results of the study showed that the new controller provided good response reduction in a broad range of near fault earthquake excitations. In this paper, the authors investigate the seismic performance of a new semiactive variable damping device, namely semiactive independently variable damper (SAIVD). This device consists of four linear visco-elastic elements, commonly known as Kelvin–Voigt or simply Kelvin elements, arranged in a rhombus configuration. The level of damping force is varied through an appropriate positioning of the arms of the device. The main advantage of this device is that it is essentially linear, simple to construct, and does not present the difficulties commonly associated with working with nonlinear devices (e.g. friction). The primary goal of this paper is to (i) introduce and experimentally verify a new variable damping device capable of varying the level of damping force smoothly, (ii) study the performance of the $H_\infty$ control algorithm and the semiactive device to achieve response reductions in smart base isolated buildings in a set of near-fault earthquakes, and (iii) compare the seismic performance of the newly developed variable damping SAIVD device and the variable friction SAIVF device.

The most popular semiactive variable damping device is the Magnetorheological (MR) damper. This device has been studied extensively [7, 8, 21, 23, 24] and shown to be effective in reducing the response of base isolated structures. The magnitude of damping force in a MR damper is a nonlinear function of voltage and velocity across the damper. The variation in the damping is achieved by changing the voltage input to the damper. Several nonlinear hysteretic models [25] have been proposed to describe the force–velocity relationship of the MR damper. Though the proposed models describe the behaviour of the damper well, the nonlinear nature of the analytical models complicates modelling and controller design. Furthermore, it has been shown that the nonlinear dampers may result in increased floor accelerations and shears in base isolated buildings in certain earthquakes [26]. In contrast, linear viscous dampers can easily be modelled, and the relative simplicity of these devices makes them an attractive alternative to nonlinear devices.

MR Dampers have been used in conjunction with a host of control algorithms, e.g. clipped optimal control [21, 23, 24], and Lyapunov control [8]. A majority of the control algorithms developed result in on–off switching laws. Though these algorithms are effective in reducing base displacements, in many cases the benefits are achieved at the cost of increase in floor accelerations and inter-storey drifts. The increase in the super-storey accelerations and inter-storey drifts are a result of the abrupt switching; smooth switching algorithms alleviate the problem to a large extent [5, 22].

Robust control methods using $H_\infty$ and other methods based on optimal control theory have been mostly studied in the context of active control for structures [27–29]. Relatively few studies that apply $H_\infty$ to semiactive control using variable damping semiactive devices have been reported. Recently, Narasimhan *et al*. [22] developed a control algorithm based on $H_\infty$. This control algorithm was shown to be effective in reducing the response of base isolated buildings in a set of near-fault earthquakes. The algorithm uses the magnitude of the optimal force calculated based on



DOI: 10.1002/eqe

an on-line $H_\infty$ controller and this information is used to calculate the optimum position of the semiactive device. The frequency information of the excitation is incorporated into the controller formulation using a higher order filter that captures the peak spectral characteristics of the near fault earthquakes. The algorithm results in a smooth variation of the level of semiactive force; hence, eliminates some of the disadvantages associated with rapidly switching devices.

In this paper, a semiactive variable damping device, SAIVD, is developed. The new variable damping device consists of four Kelvin elements arranged in a rhombus configuration. The stiffness elements are so chosen that they act only to restore the position of the device and their contribution to the overall system stiffness is negligible. The control action is achieved by adjusting the angle of the arms of the device, or the aspect ratio of the rhombus configuration, resulting in a smooth variation of the semiactive force. This type of semiactive force variation eliminates the disadvantages associated with rapid switching devices. The main advantage of this device is that it is essentially linear, simple to construct, and does not present the difficulties commonly associated with modelling nonlinear devices (e.g. friction). Experimental results are presented to verify the proposed analytical model of the device. The central idea of the control algorithm is to determine the position of SAIVD based on the optimal force generated by the $H_\infty$ controller. The $H_\infty$ controller is designed using appropriate input (excitation) and output (response) frequency-dependent weighting filters for optimal performance in reducing near-fault earthquake responses. The results of the performance of the SAIVD control are compared with the results from the SAIVF device from the previous study, and the relative merits are discussed.

## 2. STRUCTURE WITH VARIABLE DAMPING SYSTEM: FORMULATION

The structure used for the numerical simulations is a planar five-storey base isolated building, with one degree-of-freedom per floor, resulting in a total of six degrees of freedom. The state space equations for the six degrees of freedom smart base isolated structure shown in Figure 1 is as follows:

$$\dot{\mathbf{x}}(t) = \mathbf{A}\mathbf{x}(t) + \mathbf{B}u(t) + \mathbf{E}\ddot{U}_{\mathrm{g}}(t) \tag{1}$$

where $\mathbf{x}$ consists of the states, $u(t) = f_{\mathrm{d}}(t)$ is the time-varying semiactive control device force, $\ddot{u}_{\mathrm{g}}(t)$ is the ground acceleration and $\mathbf{A}$, $\mathbf{B}$ and $\mathbf{E}$ are system matrices that are defined as follows:

$$\mathbf{A} = \begin{bmatrix} \mathbf{0} & \mathbf{I} \\ -\mathbf{M}^{-1}\mathbf{K} & -\mathbf{M}^{-1}\mathbf{C} \end{bmatrix}, \quad \mathbf{B} = \begin{bmatrix} \mathbf{0} \\ \mathbf{M}^{-1}\boldsymbol{\Lambda} \end{bmatrix}, \quad \mathbf{E} = -\begin{bmatrix} \mathbf{0} \\ \boldsymbol{\Gamma} \end{bmatrix}$$

In the above equations, $\mathbf{M}$ is a diagonal mass matrix formed using 6800 kg for the mass of the base and 5897 kg for the remaining five floors. The damping coefficients for the base and the five stories are 7480, 67 000, 58 000, 57 000, 50 000 and 38 000 N s/m, respectively. The stiffness of the base is 231.5 kN/m and the stiffness of the five stories are 33 732, 29 093, 28 621, 24 954 and 19 059 kN/m, respectively. The location of the devices and earthquake influence vector are represented by, $\Lambda = [1\ 0\ 0\ 0\ 0\ 0]^{\mathrm{T}}$ and $\Gamma = [1\ 1\ 1\ 1\ 1\ 1]^{\mathrm{T}}$. The natural frequencies of the base isolated structure are 0.40, 5.46, 10.27, 14.67, 18.3 and 21.3 Hz, respectively. The damping in the isolation system is so chosen to provide a damping ratio of 4% in the isolated case for the fundamental mode. The earthquakes used in this study are 1994 Northridge—Newhall (Fault-Normal 360 and Fault-Parallel 90), Sylmar (Fault-Normal 360 and Fault-Parallel 90) and Rinaldi



DOI: 10.1002/eqe

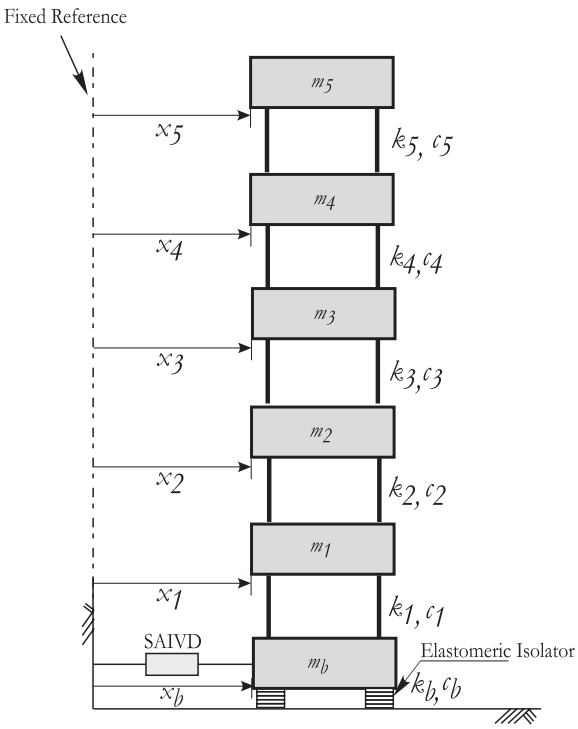


Figure 1. Five storey building model with SAIVD.

(Fault-Normal 228 and Fault-Parallel 318) components, 1995 Kobe earthquake (JMA East–West and North–South), 1999 Jiji earthquake(068 East–West and North–South) and 1992 Erzikan (East–West and North–South) earthquake.

## 3. SEMIACTIVE VARIABLE DAMPING DEVICE (SAIVD)

The semiactive independently variable damper (SAIVD) is motivated by the semiactive variable stiffness device (SAIVS) [4, 30], and the semiactive variable friction device (SAIVF) [22]. However, unlike the SAIVF device, the SAIVD is linear in all its major components. The SAIVD device consists of four Kelvin elements, arranged in a rhombus configuration as shown in Figure 2. A scaled version of the device that is used for the experimental study is shown in Figure 3. The spring-dashpot elements are connected to joints 1 to 4 as shown in Figure 2. As in the SAIVS and SAIVF devices, the joint 1 is fixed in the $x$ direction and can be positioned in the $y$ direction by a linear electromechanical actuator and controller. Joint 2 is free to move in both the $x$ and $y$ directions. Joints 3 and 4 are free to move only in the $x$ direction. The ends of the guide rail, on which joint 2 moves, are attached to the base slab. The ends of the guide rail, on which joints 3 and 4 move are attached to the foundation. The electromechanical actuator is fixed to the foundation and can actuate in the $y$ direction thus moving joint 1 to the required position. The linear electromechanical actuator configures the aspect ratio of the rhombus configuration of SAIVD device. The aspect ratio changes between the fully closed (joint 1 and 2 are in the



DOI: 10.1002/eqe

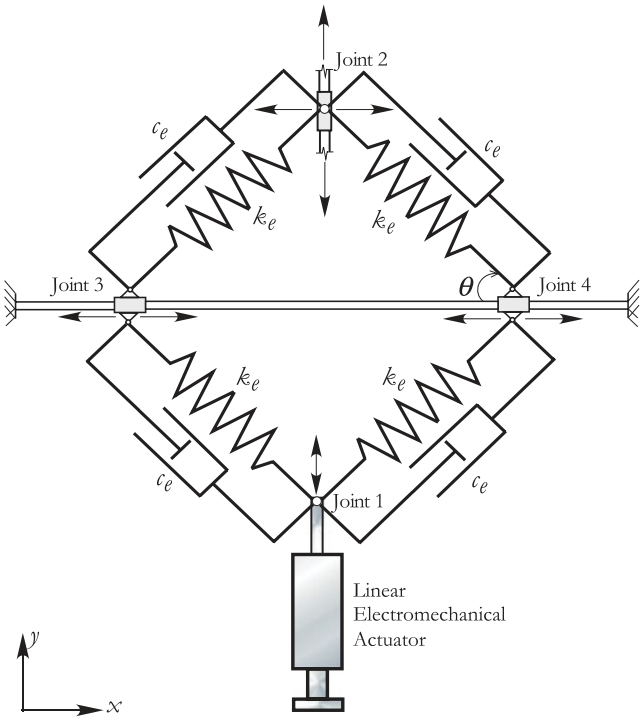


Figure 2. Analytical model of the variable friction device.

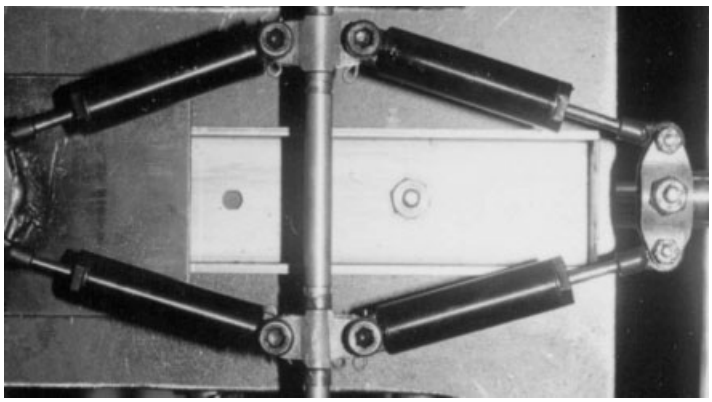

Figure 3. Scaled model of SAIVD used for the experimental study.

closest position) and open configurations (joints 3 and 4 are in the closest position) leading to maximum and minimum stiffness, respectively. A control algorithm and controller are used to regulate the linear electromechanical actuator. The power required by the actuator to change the aspect ratio of the device is nominal. Each of the pair of elements are located at an angle, $\theta$ to the horizontal. The stiffness elements act as restoring devices and their contribution to the overall system stiffness (stiffness of the elastomeric isolation system) is negligible. The SAIVD device is



DOI: 10.1002/eqe

capable of providing smooth variation of the level of damping force by varying the angle ($\theta$) of the arms of the device. The magnitude of force developed in the device is a function of the angle, $\theta$, given by

$$f_d(t) = k_e f(\theta, t)^2 y_d(t) + c_e v(t) f(\theta, t) \tag{2}$$

where $y_d(t)$ is the displacement in the $x$ direction at joint 2, $v(t)$ is the velocity at joint 2, $k_e$ is the stiffness of single spring, $\theta(t)$ is the time varying angle of the spring elements with the horizontal for any given device position, and $c_e$ is a constant. Note $f$ needs to squared in the right hand side of Equation (2), similar to the first term; however, comparison with experimental results lead to the use of $f$ without being squared. The angle, $\theta$ can only vary between angles 0 and $\pi/2$. The time-varying function $f(\theta)$ is the cosine of angle $\theta$ and given by

$$f(\theta, t) = \cos\ \theta(t) [0 \leqslant \theta \leqslant \pi/2] \tag{3}$$

## 4. SCALED MODEL EXPERIMENT

An experimental study was conducted in order to determine the force characteristics of the device and provide validation to the proposed analytical model. A scaled model of the SAIVD was tested

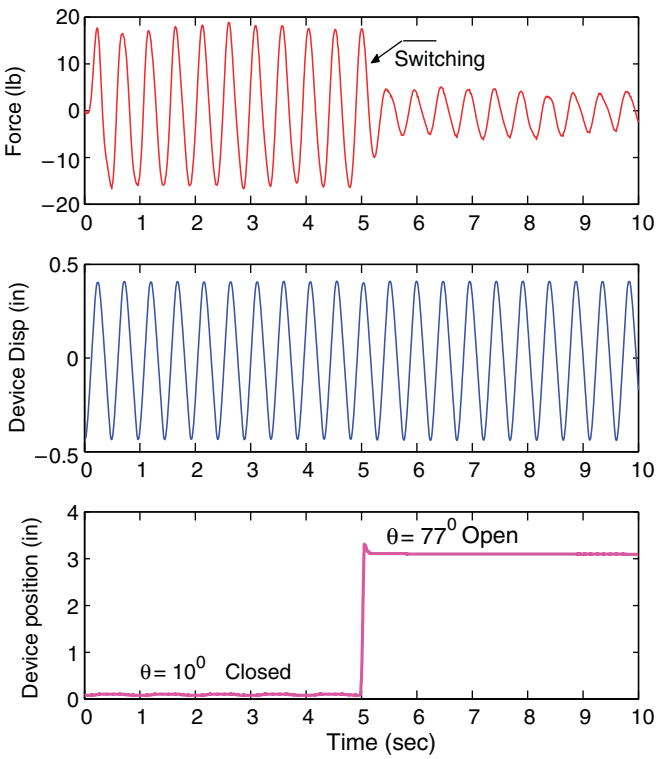


Figure 4. Experimental results—force developed in the SAIVD device excited by a 2.0 Hz sinusoid with an amplitude of 0.40 in.



DOI: 10.1002/eqe

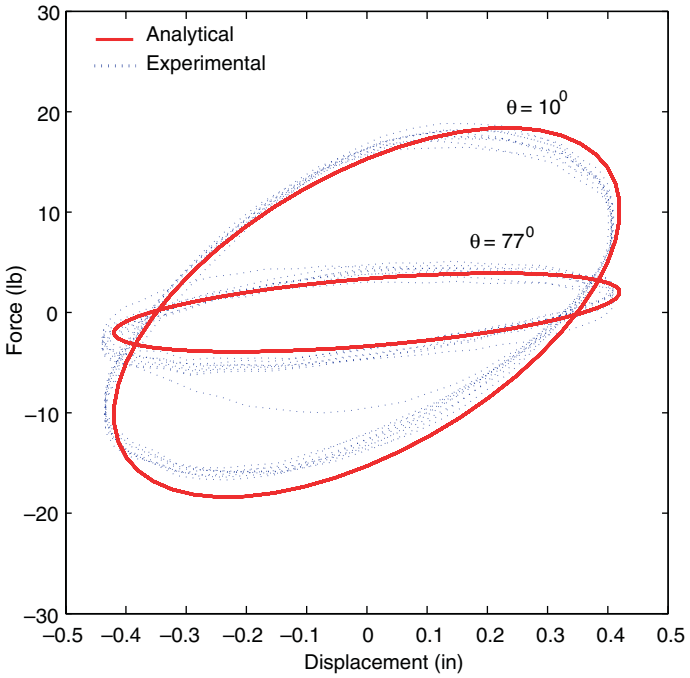


Figure 5. Comparison of experimental and analytical results for SAIVD device.

for two representative positions achieved through switching in real-time during the course of the experiment. The scaled SAIVD model used for the experimental study is shown in Figure 3. A 2.0 Hz sinusoidal excitation was used to generate the force required to determine the force–displacement relationship for the device. The magnitude of the force in the device for two positions, $\theta = 10°$ (closed), and $\theta = 77°$ (open), are shown in Figure 4. The response of the device to real-time switching is also shown at $t = 5$ s, when the device is switched from a state of higher damping to one of lower value, while continually excited by the sinusoid.

Figure 5 shows the comparison of experimental and simulated force–displacement relationship for the variable damping device at two positions of the angle $\theta$. Equation (2) is used to simulate the force corresponding to the device positions measured in the experiment. The comparison study shows that the analytical model for the device provides a good representation of the force generated by the SAIVD device. The simulated full-scale force–displacement relationship for the SAIVD device used in the simulation study is shown in Figure 6 for various positions of $\theta$.

## 5. $H_\infty$ SEMIACTIVE CONTROL ALGORITHM

The semiactive control algorithm consists of two steps: (1) develop a primary $H_\infty$ controller based on the linear time-invariant uncontrolled structure characteristics, and (2) calculate the position of the SAIVD device at each time instant based on the results obtained in step 1. The details of the algorithm are explained in the following section.



DOI: 10.1002/eqe

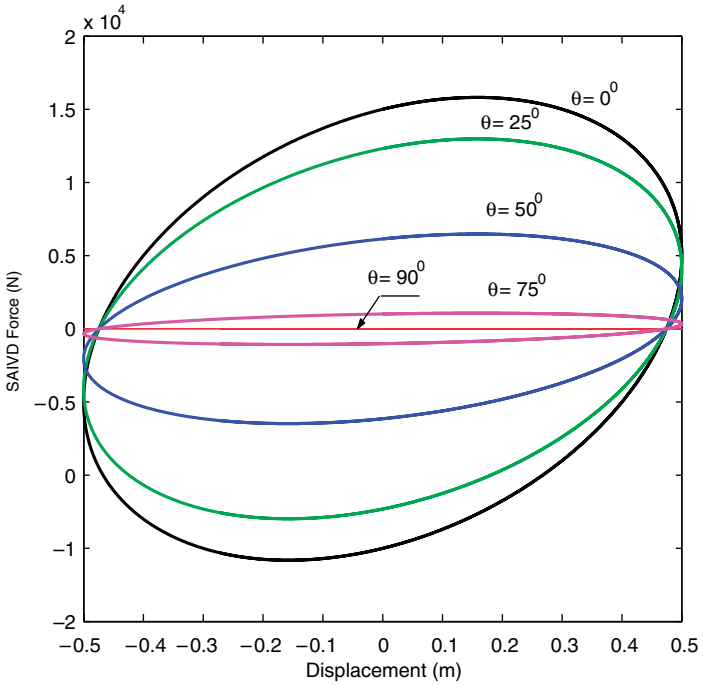


Figure 6. Force generated in the SAIVD device used in the simulation study due a harmonic excitation of $\omega = 1$ rad/s.

### 5.1. *Design of the primary $H_\infty$ controller*

For the design of the primary $H_\infty$ controller, the generalized equations of motion are cast in the following form [31]:

$$\dot{\mathbf{x}} = \mathbf{A}\mathbf{x} + \mathbf{B}_1\mathbf{w} + \mathbf{B}_2\mathbf{u} \tag{4}$$

$$\mathbf{z} = \mathbf{C}_1\mathbf{x} + \mathbf{D}_{11}\mathbf{w} + \mathbf{D}_{12}\mathbf{u} \tag{5}$$

$$\mathbf{y} = \mathbf{C}_2\mathbf{x} + \mathbf{D}_{21}\mathbf{w} + \mathbf{D}_{22}\mathbf{u} \tag{6}$$

where $\mathbf{z}$ are the regulated outputs, $\mathbf{y}$ are the measurements, $\mathbf{x}$ are the states, $\mathbf{B}_1$, $\mathbf{B}_2$ and $\mathbf{C}_1$, $\mathbf{C}_2$, $\mathbf{D}_{11}$, $\mathbf{D}_{12}$, $\mathbf{D}_{21}$, $\mathbf{D}_{22}$ are mapping matrices of appropriate dimensions. $\mathbf{w}$ and $\mathbf{u}$ contain the external disturbance and control forces, respectively.

The solution for the controller for the generalized regulator problem [32–36] is given by

$$\mathbf{u} = -\mathbf{F}_\infty\hat{\mathbf{x}} \tag{7}$$

and the state estimator is given by

$$\dot{\hat{\mathbf{x}}} = \mathbf{A}\hat{\mathbf{x}} + \mathbf{B}_2\mathbf{u} + \mathbf{B}_1\hat{\mathbf{w}} + \mathbf{J}_\infty\mathbf{L}_\infty(\mathbf{y} - \hat{\mathbf{y}}) \tag{8}$$



DOI: 10.1002/eqe

where

$$\hat{\mathbf{w}} = \gamma^{-2}\mathbf{B}_1'\mathbf{K}_\infty\hat{\mathbf{x}}$$

$$\hat{\mathbf{y}} = \gamma^{-2}\mathbf{D}_{21}\mathbf{B}_1'\mathbf{K}_\infty\hat{\mathbf{x}} + \mathbf{C}_2\hat{\mathbf{x}}$$

$$\mathbf{F}_\infty = (\mathbf{D}_{12}'\mathbf{D}_{12})^{-1}(\mathbf{B}_2'\mathbf{K}_\infty + \mathbf{D}_{12}'\mathbf{C}_1)$$

$$\mathbf{L}_\infty = (\mathbf{N}_\infty\mathbf{C}_2' + \mathbf{B}_1\mathbf{D}_{21}')(\mathbf{D}_{21}\mathbf{D}_{12}')^{-1}$$

and

$$\mathbf{J}_\infty = (\mathbf{I} - \gamma^{-2}\mathbf{N}_\infty\mathbf{K}_\infty)^{-1}$$

The term, $\hat{\mathbf{w}}$ and $\hat{\mathbf{y}}$ are the estimates of the worst case disturbance and output of the estimator. There exists a stabilizing controller if and only if there exists positive semidefinite solutions to the two Riccatti equations for $\mathbf{K}_\infty$ and $\mathbf{N}_\infty$ and the condition

$$\rho(\mathbf{K}_\infty\mathbf{N}_\infty) < \gamma^2 \tag{9}$$

where $\rho(A)$ is the spectral radius of $A$ which is defined as the largest singular value of $A$.

The terms, $\mathbf{K}_\infty$ and $\mathbf{N}_\infty$ are the solutions to the controller and estimator Riccati equations given by

$$\mathbf{K}_\infty = \mathrm{Ric}\begin{pmatrix} \mathbf{A} - \mathbf{B}_2\tilde{\mathbf{D}}_{12}\mathbf{D}_{12}'\mathbf{C}_1 & \gamma^{-2}\mathbf{B}_1\mathbf{B}_1' - \mathbf{B}_2\tilde{\mathbf{D}}_{12}\mathbf{B}_2' \\ -\tilde{\mathbf{C}}_1'\tilde{C}_1 & -(\mathbf{A} - \mathbf{B}_2\tilde{\mathbf{D}}_{12}\mathbf{D}_{12}'\mathbf{C}_1)' \end{pmatrix} \tag{10}$$

$$\mathbf{N}_\infty = \mathrm{Ric}\begin{pmatrix} (\mathbf{A} - \mathbf{B}_1\mathbf{D}_{21}\tilde{\mathbf{D}}_{21}\mathbf{C}_2)' & \gamma^{-2}\mathbf{C}_1'\mathbf{B}_1 - \mathbf{C}_2'\tilde{\mathbf{D}}_{21}\mathbf{C}_2 \\ -\tilde{\mathbf{B}}_1\tilde{\mathbf{B}}_1' & -(\mathbf{A} - \mathbf{B}_1\tilde{\mathbf{D}}_{21}'\tilde{\mathbf{D}}_{21}\mathbf{C}_2) \end{pmatrix} \tag{11}$$

where

$$\tilde{\mathbf{C}}_1 = (\mathbf{I} - \mathbf{D}_{12}\tilde{\mathbf{D}}_{12}\mathbf{D}_{12}')\mathbf{C}_1$$

$$\tilde{\mathbf{B}}_1 = \mathbf{B}_1(\mathbf{I} - \mathbf{D}_{21}'\tilde{\mathbf{D}}_{21}\mathbf{D}_{21})$$

$$\tilde{\mathbf{D}}_{12} = (\mathbf{D}_{12}'\mathbf{D}_{12})^{-1}, \quad \tilde{\mathbf{D}}_{21} = (\mathbf{D}_{21}\mathbf{D}_{21}')^{-1}$$

In order to enhance the performance of the primary controller, the frequency information of the earthquake excitation and the desired output control are added to the state-space equations in Equations (4)–(6) through state-space augmentation. The earthquake excitation filter, whose output has the frequency peak corresponding to the maximum energy in a set of near-fault earthquakes, and input is white, is described by the transfer function [22]

$$F(s) = \frac{8\zeta_g^2\omega_g^2 s^2}{[s^2 + 2\zeta_g\omega_g s + \omega_g^2]^2} \tag{12}$$

where $\omega_g = 2\pi$ rad/s and $\zeta_g = 0.3$. The outputs are weighted using a first order filter of the form, $W = a/s + a$, where, $a = 3.5$ rad/s, which determines the roll-off frequency. Since the objective



DOI: 10.1002/eqe

is to regulate the fundamental mode responses of the structure, a first order filter is used in the controller design. The input excitation filter can be written in the state-space form as

$$\begin{aligned} \dot{\mathbf{x}}_\mathrm{f} &= \mathbf{A}_\mathrm{f}\mathbf{x}_\mathrm{f} + \mathbf{B}_\mathrm{f} w \\ \ddot{U}_\mathrm{g} &= \mathbf{C}_\mathrm{f}\mathbf{x}_\mathrm{f} \end{aligned} \tag{13}$$

where $w$ is the white noise excitation, $\mathbf{x}_\mathrm{f}$ are the states of the input filter. The output weighting filter can be written in the state-space form as

$$\dot{\mathbf{x}}_\mathrm{o} = \mathbf{A}_\mathrm{o}\mathbf{x}_\mathrm{o} + \mathbf{B}_\mathrm{o}\mathbf{x} \tag{14}$$

$$\mathbf{z}_\mathrm{o} = \mathbf{C}_\mathrm{o}\mathbf{x}_\mathrm{o} \tag{15}$$

where $\mathbf{x}_\mathrm{o}$ are the states of the output filter, $\mathbf{A}_\mathrm{o}$, $\mathbf{B}_\mathrm{o}$, and $\mathbf{C}_\mathrm{o}$ are the system matrices.

The augmented state-space equations can now be written as

$$\dot{\mathbf{x}}_\mathbf{a} = \mathbf{A}_\mathbf{a}\mathbf{x}_\mathbf{a} + \mathbf{B}_\mathbf{a1}\mathbf{w}_\mathbf{a} + \mathbf{B}_\mathbf{a2}u \tag{16}$$

$$\mathbf{z}_\mathbf{a} = \mathbf{C}_\mathbf{a1}\mathbf{x}_\mathbf{a} + \mathbf{D}_\mathbf{a11}\mathbf{w}_\mathbf{a} + \mathbf{D}_\mathbf{a12}u \tag{17}$$

$$\mathbf{y}_\mathbf{a} = \mathbf{C}_\mathbf{a2}\mathbf{x}_\mathbf{a} + \mathbf{D}_\mathbf{a21}\mathbf{w}_\mathbf{a} + \mathbf{D}_\mathbf{a22}u \tag{18}$$

where $\mathbf{z}_\mathbf{a}$ are the regulated outputs, $\mathbf{y}_\mathbf{a}$ are the measurements, $\mathbf{x}_\mathrm{a} = [\dot{\mathbf{x}}\ \dot{\mathbf{x}}_\mathrm{f}\ \dot{\mathbf{x}}_\mathrm{o}]^\mathrm{T}$, $\mathbf{B}_\mathbf{a1} = [\mathbf{0}\ \mathbf{B}_f\ \mathbf{0}]^\mathrm{T}$, $\mathbf{B}_\mathbf{a2} = [\mathbf{B}\ \mathbf{0}\ \mathbf{0}]^\mathrm{T}$ and $\mathbf{C}_\mathbf{a1}$, $\mathbf{C}_\mathbf{a2}$, $\mathbf{D}_\mathbf{a11}$, $\mathbf{D}_\mathbf{a12}$, $\mathbf{D}_\mathbf{a21}$, $\mathbf{D}_\mathbf{a22}$ are mapping matrices of appropriate dimensions. In the control formulation, the regulated outputs contain the inter-storey drifts and the total accelerations of all floors, written as $[\mathbf{x}_\mathrm{b}, \mathbf{x}_i - \mathbf{x}_{i-1}, \ddot{\mathbf{x}}_\mathrm{b}, \ddot{\mathbf{x}}_i]$, where $i$ corresponds to the floor number, $1, 2, \ldots, 5$. The measured outputs for the $H_\infty$ controller formulation contain the foundation acceleration, the base acceleration, and total accelerations of all floors, written as $[\ddot{U}_\mathrm{g}, \ddot{\mathbf{x}}_\mathrm{b}, \ddot{\mathbf{x}}_i]$, where $i$ corresponds to the floor number. The external disturbance, $w = \ddot{U}_\mathrm{g}$ is augmented to contain both the external disturbance and the measurement noise and is contained in the vector, $\mathbf{w}_\mathbf{a} = [\ddot{U}_\mathrm{g}, \mathbf{v}]^\mathrm{T}$, where $\mathbf{v}$ is the measurement noise. Additionally, the device displacement, $y_\mathrm{d}$, is also measured for the control algorithm. However, this measurement is not used in the $H_\infty$ controller formulation. Readers are referred to the earlier paper by the authors [22] for more detailed discussion on the augmentation procedure and the filter design.

### *5.2. Design of the semiactive controller*

The device position is determined from Equation (7) by equating the force in the SAIVD device to the optimal force generated by the $H_\infty$ controller. The resulting equations to determine the unknown variable $f(\theta, t)$ can be written as

$$f_\mathrm{d}(t) = k_\mathrm{e} f(\theta, t)^2 y_\mathrm{d}(t) + c_\mathrm{e} v f(\theta, t) = -\mathbf{F}_\infty \hat{\mathbf{x}}_\mathrm{a} = F_\infty \tag{19}$$

Solving the above equation for the device position, $f(\theta, t)$, results in the following:

$$f(\theta, t) = \frac{-c_\mathrm{e} v \pm \sqrt{c_\mathrm{e}^2 v^2 + 4 y_\mathrm{d} F_\infty k_\mathrm{e}}}{2 k_\mathrm{e} y_\mathrm{d}} \tag{20}$$



DOI: 10.1002/eqe

Due to the physical characteristics of the SAIVD device, the value of $f(\theta, t)$ is positive and bounded between 0 and +1. The maximum of the two quadratic roots for Equation (20) are chosen and hence, Equation (20) can be written as

$$\hat{f}(\theta, t) = \max |f(\theta, t)| \tag{21}$$

In order to prevent numerical difficulties, $y_d = 0.01$ m when the magnitude of the base displacement, $|y_d| \leqslant 0.01$ m. The values obtained by Equation (21) is passed through a low pass filter to alleviate the high frequency switching, and the resulting control law can be written as

$$\hat{f}_c(\theta, t) = \begin{cases} \hat{f}_{cm} & (v \geqslant 1) \\ v & \\ 0 & (v \leqslant 0) \end{cases} \tag{22}$$

where $v$ is the output of the following first order filter:

$$\dot{v} = -a_1 v + a_2 \hat{f}(\theta, t) \tag{23}$$

The values of $a_1$ and $a_2$ in the above equation are assumed to be 10.0 rad/s, $c_1 = 30\,000$ N s/m and $k_e = 15\,000$ N/m. The value of $\hat{f}_{cm}$ is 1 or 0.87 depending on the desired maximum control force (discussed in more detail in the following section).

## 6. RESULTS AND DISCUSSION

The results of the simulation study for the structure for the uncontrolled case (no active or semiactive devices), and for the case of $H_\infty$ active control have been presented in a recent paper by the authors [22]. It was shown in the aforementioned paper that the semiactive control using SAIVF device performs well in reducing the responses of the structure for near-fault earthquakes. It was evident from the study that the semiactive control using SAIVF device was effective in reducing the structural forces and accelerations while achieving the same level of reductions in the peak base displacements as the case with passive control (device is set at the position that generated the maximum force). The main objective of the current study is to study the performance of the newly developed SAIVD device for a set of near-fault earthquake excitations. In the first step, the performance of the SAIVD device considered in the current study is compared with the results of the previous study using the SAIVF device [22] to investigate the relative advantages of the two newly developed semiactive devices. Then, the performance of the semiactive controller is presented and a comparison to the passive case is discussed.

A set of nine performance indices, $J_1$ through $J_9$, shown in Table I have been used to assess the performance of the control algorithm and SAIVD device. These indices have been used to study the performance of control algorithms for base isolated buildings [37] in several earlier studies including the base isolation benchmark [26, 38]. The indices $J_1$ through $J_5$ measure the peak values of base shear, structural shear, base displacement, inter-storey drift and floor accelerations, respectively. These values are normalized by their respective uncontrolled values. In the following discussion, the term 'uncontrolled' refers to the case when there is no force feedback to the structure and the control device (active or semiactive) is disconnected from the structural system. The term



DOI: 10.1002/eqe

Table I. Performance indices.

| | | |
|---|---|---|
| Peak base shear* | Peak structure shear* | Peak base displacement* |
| $J_1 = \dfrac{\max_t \| V_0(t) \|}{\max_t \| \hat{V}_0(t) \|}$ | $J_2 = \dfrac{\max_t \| V_1(t) \|}{\max_t \| \hat{V}_1(t) \|}$ | $J_3 = \dfrac{\max_t \| x_b(t) \|}{\max_t \| \hat{x}_b(t) \|}$ |
| Peak interstory drift* | Peak floor acceleration* | Peak control force |
| $J_4 = \dfrac{\max_{t,f} \| d_f(t) \|}{\max_{t,f} \| \hat{d}_f(t) \|}$ | $J_5 = \dfrac{\max_{t,f} \| a_f(t) \|}{\max_{t,f} \| \hat{a}_f(t) \|}$ | $J_6 = \dfrac{\max_t \| f_d(t) \|}{\max_t \| V_0(t) \|}$ |
| RMS base displacement* | RMS floor acceleration* | Energy dissipated by SAIVF |
| $J_7 = \dfrac{\max_i \| \sigma_d(t) \|}{\max_i \| \sigma_{\hat{d}}(t) \|}$ | $J_8 = \dfrac{\max_f \| \sigma_a(t) \|}{\max_f \| \sigma_{\hat{a}}(t) \|}$ | $J_9 = \dfrac{[\int_0^T f_d(t) \dot{x}_b(t)\, dt]}{\int_0^T \langle V_0(t) \dot{U}_g(t) \rangle\, dt}$ |

*The denominator consists of the corresponding response quantity in the uncontrolled case $f =$ floor number, $1, \ldots, 5$; $t =$ time, $0 \leqslant t \leqslant T$; $\langle \cdot \rangle =$ inner product; $\| \cdot \| =$ vector magnitude; $V_o$, $V_1 =$ base and structural shears; $x_b =$ base displacement; $d_f =$ interstory drift; $a_f =$ floor acceleration; $\sigma_d$ and $\sigma_a =$ RMS base displacement and floor acceleration; $\hat{} =$ corresponding response quantity in the uncontrolled case.

'passive' or 'closed' refers to the position where the device generates maximum force at all times and no variation of the position of the arms of the device is undertaken during the simulation. The performance index $J_6$ measures the maximum control force developed in the device normalized by the peak base shear. The indices, $J_7$ and $J_8$ measure the RMS values of displacement and base acceleration normalized by their uncontrolled values. The index $J_9$ measures the energy dissipated by the semiactive device as a percentage of the input excitation energy.

### *6.1. Comparison of the performance of SAIVD and SAIVF in near fault earthquakes*

One of the main objectives of this study is a comparison of the performance of the newly developed variable damping device, SAIVD and the variable friction device, SAIVF [22]. In order to accomplish this, the performance of the two devices are compared under similar magnitudes of peak semiactive control force for the suite of earthquake excitations considered in this study. The quantity, $\hat{f}_{cm}$ in Equation (22) is treated as a variable and the optimum value of $\hat{f}_{cm}$ is determined by a minimization of the difference between the peak control force of SAIVD and SAIVF devices for the passive case. Alternatively, the optimum value for the comparison study is the value of $\hat{f}_{cm}$ in the SAIVD device that results in similar magnitude of the peak control force as in the SAIVF device for the range of earthquake excitations considered. Specifically, the 2-norm of the vector (because all the earthquakes are considered in finding the minimum) difference in the performance index, $J_6$ denoted by $\| \delta_{J_6} \|_2$ for the two cases is used to determine $\hat{f}_{cm}$. In doing so, it is recognized that the conclusions regarding the relative performance between the two devices can be drawn under similar peak semiactive control force magnitudes for the two devices for the suite of earthquakes under consideration. Figure 7 shows the results of the optimization study to determine $\hat{f}_{cm}$ that minimizes the difference in the normalized peak control force (given by the performance index, $J_6$), for both cases. This value corresponds to a position of SAIVD device, $\hat{f}_{cm} = 0.87$. This value is used in Equation (22) for the comparison study.

Figures 8 and 9 show a comparison of the semiactive control with SAIVD and SAIVF devices in terms of the performance indices as a function of the peak ground acceleration, normalized by



DOI: 10.1002/eqe

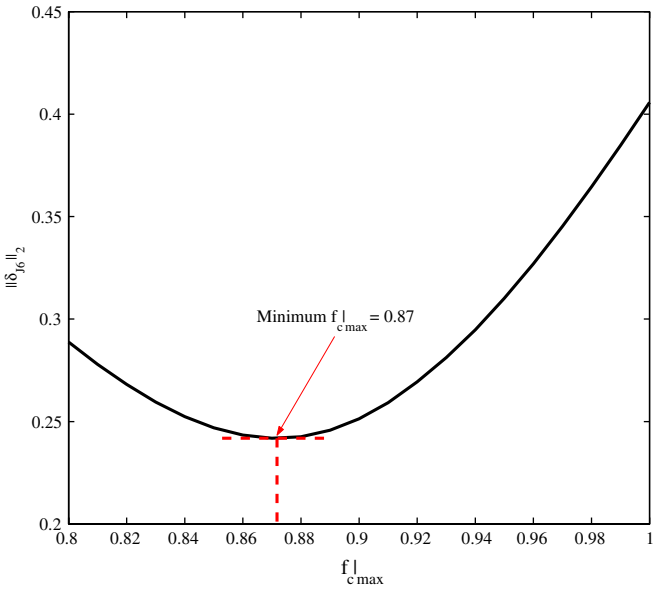


Figure 7. Determination of $\hat{f}_{cm}$ that yields a minimum value of the 2-norm of the difference of the performance index $J_6$ between SAIVF and SAIVD ($\|\delta_{J_6}\|_2$) corresponding to the passive case.

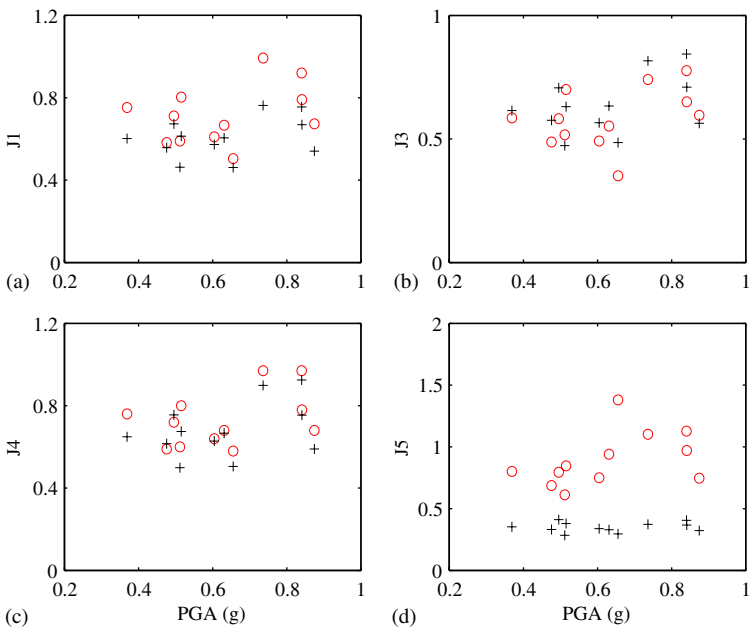


Figure 8. Peak performance indices for SAIVD (+) and SAIVF (○): (a) peak base shear ($J_1$); (b) peak base displacement ($J_3$); (c) peak inter-storey drift ($J_4$); and (d) peak floor acceleration ($J_5$).



DOI: 10.1002/eqe

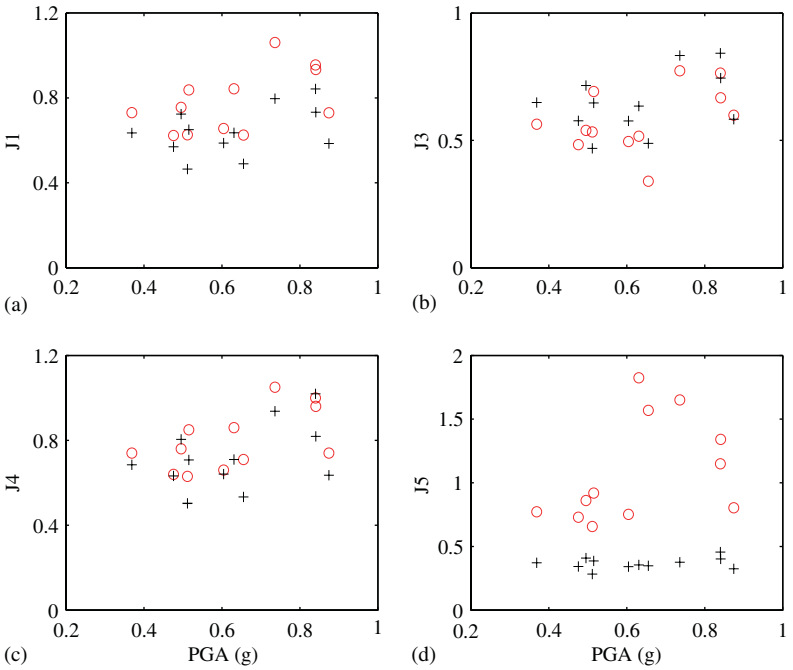


Figure 9. Peak performance indices for maximum control force passive case corresponding to SAIVD (+) and SAIVF (○): (a) peak base shear ($J_1$); (b) peak base displacement ($J_3$); (c) peak inter-storey drift ($J_4$); and (d) peak floor acceleration ($J_5$).

the acceleration due to gravity. Figure 8 shows the results for both cases when the $H_\infty$ control algorithm is used to determine the optimum position of the devices as described in the earlier sections (maximum force not to exceed the force corresponding to $\hat{f}_{cm} = 0.87$ at any time instant). Figure 9 shows the results of the corresponding passive cases, when the position of the SAIVD device is kept constant in order to generate the maximum force at all times (corresponding to $\hat{f}_{cm} = 0.87$).

From Figures 8 and 9, a predominant characteristic of the SAIVD control is the relatively uniform reduction in the peak floor accelerations ($J_5$) compared to SAIVF device for all earthquake excitations considered. It is evident that the reduction in the floor accelerations with semiactive control using SAIVF device is dependent on the excitation characteristics, whereas the control using SAIVD device is relatively independent of the excitation (for the earthquakes considered). Also, SAIVD control offers slightly better performance in terms of reducing the base shear compared to SAIVF case. SAIVF provides slightly better performance in reducing the peak base displacements compared to SAIVD. The performance of both SAIVD and SAIVF are comparable in terms of reducing peak inter-storey drifts.

Figure 10 shows the inter-storey drifts and the peak floor acceleration profiles (at different floors) for the controlled cases of SAIVD and SAIVF device for the fault-normal components of Newhall and Sylmar records from Northridge earthquake, the east–west component from Kobe-JMA earthquake, and the fault-normal component from Jiji earthquake. The results clearly show



DOI: 10.1002/eqe

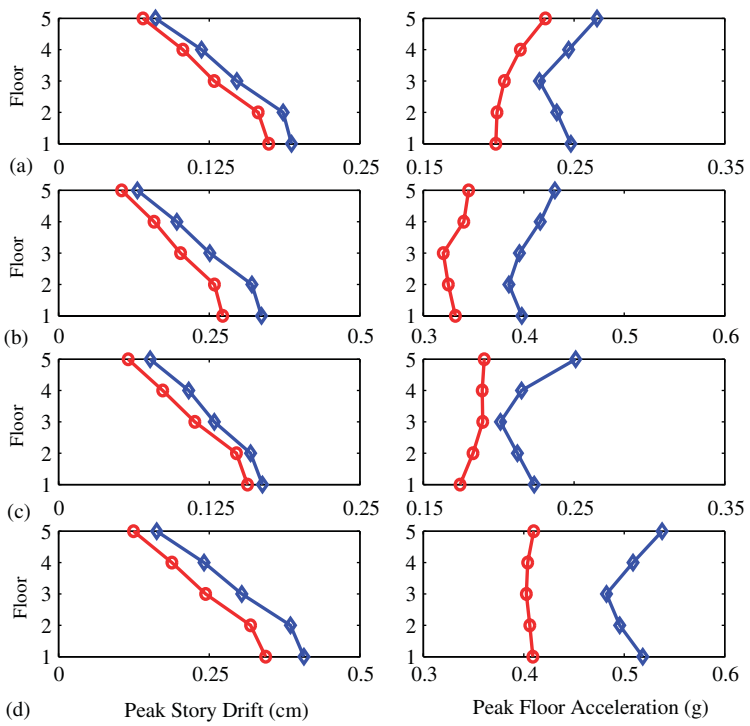


Figure 10. Comparison of inter-storey drifts and peak floor accelerations for the SAIVD (-○-) and SAIVF (-◇-) device for: (a) Newhall—FN; (b) Sylmar—FN; (c) Kobe—NS; and (d) Jiji—FN.

that the SAIVD device provides good response reductions compared to the SAIVF device for both the inter-storey drifts and the peak floor accelerations. It is also observed that the peak floor accelerations for all floors are reduced uniformly in the case of the SAIVD control.

Figure 11 shows the comparison of the peak base displacement spectra and peak 5th floor acceleration spectra for the SAIVF and SAIVD devices when excited by periodic excitation of varying frequencies. As noted previously, SAIVF device is slightly more effective in reducing the base displacement; however, compared to the SAIVF device, better performance in reducing the peak 5th floor acceleration is achieved using the SAIVD device especially at higher frequencies and higher modes.

### *6.2. Simulation results using SAIVD*

Tables II and III show the results of the simulation using SAIVD device. The performance indices for the passive case are presented in Table II. In these simulations, the passive case corresponds to $\hat{f}_{\mathrm{cm}} = 1.0$ in Equation (22) and this value is unchanged during the simulations. The performance indices for the semiactive case are presented in Table III. For this case, the maximum force generated by the $H_\infty$ control algorithm is set not to exceed the maximum physically realizable force in the SAIVD device corresponding to $\hat{f}_{\mathrm{cm}} = 1.0$. A total of 12 records from six near-fault earthquakes are used in this analytical study. The performance indices are normalized to yield



DOI: 10.1002/eqe

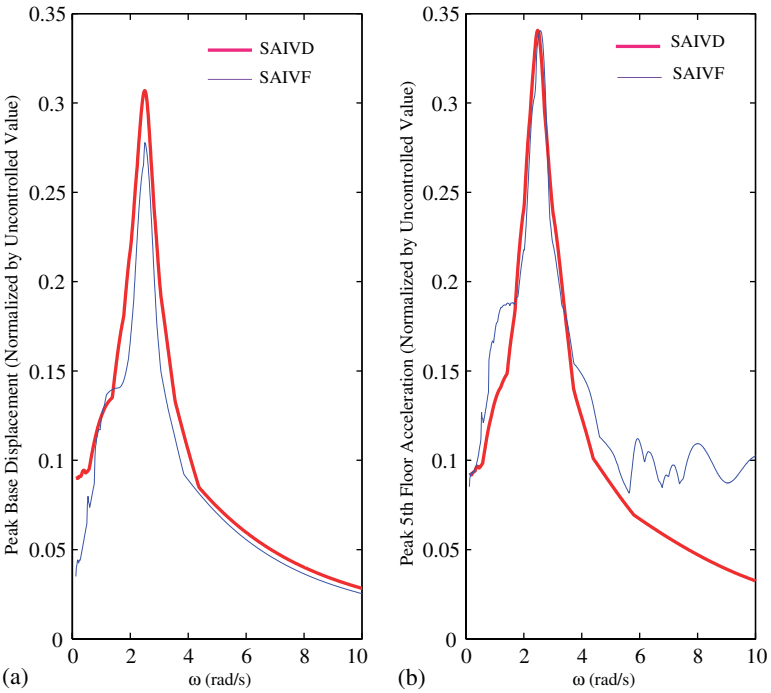


Figure 11. Frequency response comparisons for the cases of: (a) peak base displacement; and (b) peak 5th floor acceleration, for the SAIVD and SAIVF devices.

Table II. Results for the case of maximum damping—passive.

| Earthquake | Case | $J_1$ | $J_2$ | $J_3$ | $J_4$ | $J_5$ | $J_6$ | $J_7$ | $J_8$ | $J_9$ |
|---|---|---|---|---|---|---|---|---|---|---|
| Newhall | FN | 0.80 | 0.95 | 0.79 | 0.95 | 0.39 | 0.44 | 0.71 | 0.40 | 0.80 |
| | FP | 0.48 | 0.53 | 0.41 | 0.53 | 0.36 | 0.46 | 0.38 | 0.24 | 0.80 |
| Sylmar | FN | 0.55 | 0.60 | 0.53 | 0.60 | 0.32 | 0.39 | 0.35 | 0.21 | 0.80 |
| | FP | 0.53 | 0.59 | 0.50 | 0.59 | 0.32 | 0.41 | 0.34 | 0.21 | 0.80 |
| Rinaldi | FN | 0.86 | 1.05 | 0.80 | 1.04 | 0.47 | 0.42 | 0.58 | 0.34 | 0.80 |
| | FP | 0.51 | 0.57 | 0.50 | 0.57 | 0.31 | 0.35 | 0.35 | 0.21 | 0.79 |
| Kobe | FN | 0.69 | 0.77 | 0.68 | 0.77 | 0.38 | 0.47 | 0.67 | 0.37 | 0.80 |
| | FP | 0.62 | 0.68 | 0.58 | 0.68 | 0.36 | 0.51 | 0.62 | 0.36 | 0.80 |
| Jiji | FN | 0.44 | 0.48 | 0.43 | 0.48 | 0.27 | 0.28 | 0.34 | 0.20 | 0.71 |
| | FP | 0.62 | 0.66 | 0.62 | 0.66 | 0.36 | 0.33 | 0.53 | 0.32 | 0.55 |
| Erzinkan | FN | 0.61 | 0.67 | 0.58 | 0.67 | 0.36 | 0.30 | 0.42 | 0.25 | 0.80 |
| | FP | 0.70 | 0.79 | 0.65 | 0.79 | 0.40 | 0.26 | 0.44 | 0.27 | 0.80 |



DOI: 10.1002/eqe

Table III. Results for the semiactive controlled case.

| Earthquake | Case | $J_1$ | $J_2$ | $J_3$ | $J_4$ | $J_5$ | $J_6$ | $J_7$ | $J_8$ | $J_9$ |
|---|---|---|---|---|---|---|---|---|---|---|
| Newhall | FN | 0.77 (−2.81) | 0.92 (−3.31) | 0.79 −(−0.01) | 0.92 (−3.28) | 0.38 (−3.73) | 0.36 | 0.73 | 0.39 | 0.73 |
| | FP | 0.40 (−17.73) | 0.45 (−18.31) | 0.42 −(−1.76) | 0.45 (−18.25) | 0.30 (−21.40) | 0.44 | 0.41 | 0.24 | 0.77 |
| Sylmar | FN | 0.51 (−8.61) | 0.56 (−8.39) | 0.52 (−2.51) | 0.56 (−8.41) | 0.31 (−5.29) | 0.36 | 0.37 | 0.22 | 0.77 |
| | FP | 0.53 (−1.79) | 0.58 (−0.89) | 0.50 (−0.73) | 0.58 (−0.88) | 0.32 −(−1.51) | 0.36 | 0.37 | 0.22 | 0.77 |
| Rinaldi | FN | 0.75 (−14.49) | 0.92 (−13.86) | 0.82 −(−2.42) | 0.92 (−13.84) | 0.39 (−19.79) | 0.40 | 0.60 | 0.33 | 0.75 |
| | FP | 0.50 (−1.47) | 0.55 (−2.35) | 0.51 −(−1.32) | 0.55 (−2.31) | 0.29 (−6.44) | 0.32 | 0.38 | 0.23 | 0.77 |
| Kobe | FN | 0.63 (−9.47) | 0.71 (−9.18) | 0.66 (−3.54) | 0.71 (−9.19) | 0.34 (−12.75) | 0.37 | 0.67 | 0.35 | 0.74 |
| | FP | 0.55 (−13.40) | 0.63 (−8.47) | 0.58 (−0.52) | 0.63 (−8.49) | 0.33 (−9.76) | 0.47 | 0.64 | 0.36 | 0.76 |
| Jiji | FN | 0.42 (−5.75) | 0.45 (−5.34) | 0.41 (−4.64) | 0.45 (−5.31) | 0.26 (−2.61) | 0.28 | 0.39 | 0.23 | 0.68 |
| | FP | 0.59 (−5.48) | 0.63 (−5.46) | 0.59 (−5.45) | 0.63 (−5.46) | 0.34 (−5.62) | 0.30 | 0.54 | 0.32 | 0.54 |
| Erzinkan | FN | 0.58 (−5.89) | 0.64 (−4.23) | 0.58 (−1.02) | 0.64 (−4.21) | 0.37 −(−1.65) | 0.30 | 0.44 | 0.26 | 0.77 |
| | FP | 0.64 (−10.22) | 0.71 (−10.30) | 0.66 −(−1.15) | 0.71 (−10.27) | 0.39 (−2.88) | 0.25 | 0.47 | 0.28 | 0.76 |

*Note*: % Reductions compared to passive case are given inside the brackets.




DOI: 10.1002/eqe

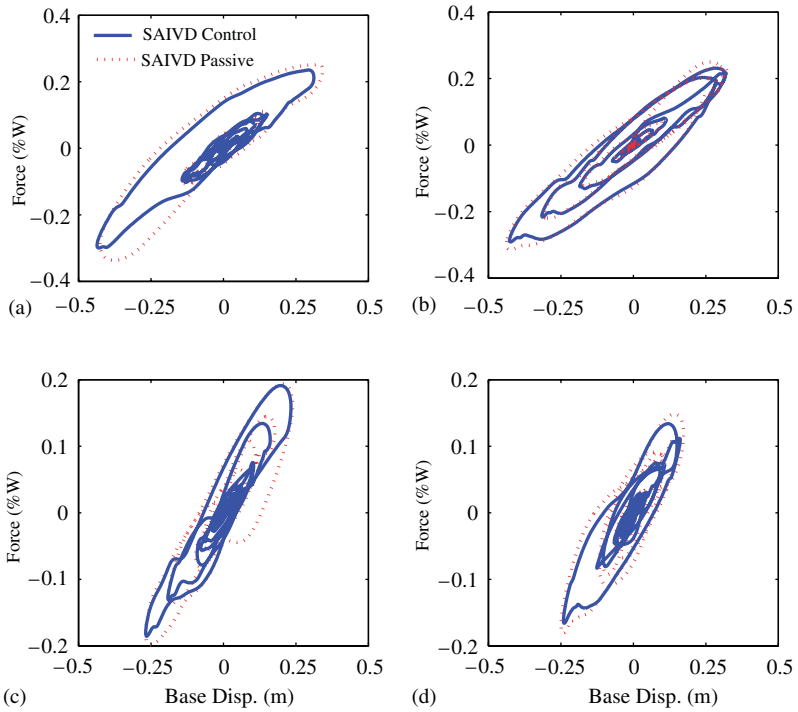


Figure 12. Total force at the isolation level *vs* base displacement for: (a) Rinaldi—FN; (b) Sylmar—FN; (c) Newhall—FN; and (d) Kobe—NS.

a value of unity corresponding to the uncontrolled case when there is no control force applied; passive or semiactive. Values less than one correspond to reductions with respect to the uncontrolled case and vice versa. In Table III, the response reduction for the corresponding performance index with respect to the passive case is shown inside the brackets next to the peak performance indices, $J_1$ through $J_5$. Reductions are denoted by a negative sign preceding the value and vice versa. The reader is referred to the earlier paper [22] by the authors for the uncontrolled values.

Figure 12 shows the relationship between the total force at the isolation level, which is the sum of the SAIVD device force and the force in the elastomeric bearings, and the base displacement for the control case for Rinaldi (FN), Sylmar (FN), Newhall (FN) and Kobe (NS) earthquakes. From the results of the semiactive control in Table III, as expected, the performance indices are all significantly less than 1. Several earlier studies have shown that higher damping results in response reductions. However, it is more interesting to discuss the performance of the controller (Table III) when compared to the results from the passive case (Table II). The base and structural shears ($J_1$ and $J_2$, respectively) for the controlled case are reduced uniformly for all earthquakes compared to the passive case. Notable reductions in the shears, of the order of 8–19%, occur for the fault-parallel components of Newhall, Erzinkan, fault-normal component of Rinaldi, and both components of Kobe. The peak base displacements for the controlled case ($J_3$) are very comparable to the passive case. The peak inter-storey drifts are reduced for the controlled case compared to the passive case for all the earthquakes. Notable reductions, of the order of 8–19%, occur for the



DOI: 10.1002/eqe

fault-parallel components of Newhall, Erzinkan, fault-normal component of Sylmar, Rinaldi and both components of Kobe. The peak floor accelerations ($J_5$) are at or below the values of their corresponding passive cases. Notable reductions, of the order of 20% occur for the fault-normal component of Rinaldi and fault-parallel component of Newhall. The RMS quantities ($J_7$ and $J_8$) are quite comparable to the passive cases. Previous research has shown that on–off type semiactive switching algorithms may result in increased base and superstructure accelerations in base isolated buildings. Results of this algorithm show that contrary to bang–bang-type controllers, the peak base and floor accelerations are reduced in all earthquakes. The new control algorithm also leads to a more efficient energy dissipation in the SAIVD device, which results in better response reductions compared to the passive case.

## 7. CONCLUSIONS

A new variable damping device, SAIVD is developed and shown to be effective in reducing the responses of a base isolated building in near fault earthquakes. The newly developed device consists of Kelvin elements in a rhombus configuration and the magnitude of the semiactive force is varied by adjusting the aspect ratio of the device. The main advantage of SAIVD device is that it is essentially linear, simple to construct, analytically model, and provides good response reductions in a suite of near fault earthquake excitations. The optimum position of the device is calculated using a $H_\infty$ algorithm. The effectiveness of the newly developed device is demonstrated by comparing it with a variable friction device, SAIVF developed in an earlier work by the authors. The results show that the SAIVD device is capable of achieving better performance in terms of reducing the peak floor accelerations while achieving similar performance in reducing the peak base displacements and shears. Results of the simulation study also indicate that the semiactive control strategy is effective for earthquakes of wide range of intensities. The nature of the new semiactive device eliminates the disadvantages associated with some abrupt switching devices and the controlled case consistently performs better than the passive case. More efficient energy dissipation in SAIVD case leads to reductions in response when compared to the passive case, indicating the effectiveness of the $H_\infty$ controller.

ACKNOWLEDGEMENTS

The authors would like to acknowledge the funding for this research provided by National Science Foundation, NSF-CAREER GRANT CMS 9996290. The support provided by the Department of Civil and Environmental Engineering, University of Waterloo, is gratefully acknowledged by the second author.

REFERENCES

1. Agrawal AK, Yang JN, He WL. Applications of some semi-active control systems for a benchmark cable-stayed bridge. *Journal of Structural Engineering* (ASCE) 2003; **129**(7):884–894.
2. He WL, Agrawal AK, Yang JN. Novel semiactive friction controller for linear structures against earthquakes. *Journal of Structural Engineering* (ASCE) 2003; **129**(7):941–950.
3. Inaudi JA. Modulated homogeneous friction: a semiactive damping strategy. *Earthquake Engineering and Structural Dynamics* 1997; **26**:361–376.
4. Nagarajaiah S, Mate D. Semi-active control of continuously variable stiffness system. *Proceedings of Second World Conference on Structural Control*, vol. 1. Wiley: New York, 1998; 397–405.



DOI: 10.1002/eqe

5. Narasimhan S, Nagarajaiah S. STFT algorithm for semiactive control of base isolated buildings with variable stiffness isolation systems subjected to near fault earthquakes. *Engineering Structures* 2005; **27**(4): 514–523.
6. Spencer BF, Nagarajaiah S. State of the art of structural control. *Journal of Structural Engineering* (ASCE) 2003; **129**(7):845–856.
7. Sahasrabudhe S, Nagarajaiah S. Experimental study of sliding isolated buildings with MR dampers. *Journal of Structural Engineering* (ASCE) 2005; **131**(7):1025–1034.
8. Sahasrabudhe S, Nagarajaiah S. Seismic response control of sliding isolated bridges with MR dampers: experimental and numerical study. *Earthquake Engineering and Structural Dynamics* 2005; **34**(7):965–983.
9. Yang JN, Wu JC, Kawashima K, Unjoh S. Hybrid control of seismic-excited bridge structure. *Earthquake Engineering and Structural Dynamics* 1995; **24**(11):1437–1451.
10. Yang JN, Kim JH, Agrawal AK. A resetting semi-active stiffness damper for seismic response control. *Journal of Structural Engineering* (ASCE) 2000; **126**(12):1427–1433.
11. Yang JN, Agrawal AK. Semi-active hybrid control systems for nonlinear buildings against near-field earthquakes. *Engineering Structures* 2002; **24**:271–280.
12. Yang JN, Wu J, Reinhorn A, Riley M. Control of sliding-isolated buildings using sliding-mode control. *Journal of Structural Engineering* (ASCE) 1996; **122**:179–186.
13. Dupont P, Kasturi P, Stokes A. Semiactive control of friction dampers. *Journal of Sound and Vibration* 1997; **202**(2):203–218.
14. Fujita *et al*. Semiactive seismic isolation system using controllable friction damper. *Bulletin of Earthquake Resistant Structure Research Center*, vol. 27, University of Tokyo, 1994.
15. Hirai J, Naruse M, Abiru H. Structural control with variable friction damper for seismic response. *Proceedings of Eleventh World Conference on Earthquake Engineering*, Paper No. 1934. Elsevier Science Ltd: Amsterdam, 1996.
16. Nishitani A, Nitta Y, Ikeda Y. Semiactive structural control based on variable slip-force level dampers. *Journal of Structural Engineering* (ASCE) 2003; **129**(7):933–940.
17. Nitsche R, Gaul L. Vibration control using semiactive friction damping. *Fifth European Control Conference ECC'99*, Karlsruhe, Germany, CDROM, 1999.
18. Stammers CW, Sireteanu T. Vibration control of machines by use of semiactive dry friction damping. *Journal of Sound and Vibration* 1998; **209**(4):671–684.
19. Wongprasert N, Symans MD. Numerical evaluation of adaptive base-isolated structures subjected to earthquake ground motions. *Journal of Engineering Mechanics* (ASCE) 2005; **131**(2):109–119.
20. Wongprasert N, Symans MD. Experimental evaluation of adaptive elastomeric base-isolated structures using variable-orifice fluid dampers. *Journal of Structural Engineering* (ASCE) 2005; **131**(6):867–877.
21. Ramallo J, Johnson EA, Spencer B. Smart base isolation systems. *Journal of Engineering Mechanics* (ASCE) 2002; **128**(10):1088–1099.
22. Narasimhan S, Nagarajaiah S. Smart base isolated buildings with variable friction systems: $H_\infty$ controller and novel SAIVF device. *Earthquake Engineering and Structural Dynamics* 2006; **35**(8):921–942.
23. Dyke SJ, Spencer Jr BF, Sain MK, Carlson JD. Seismic response reduction using magnetorheological dampers. *Proceedings of the IFAC World Congress*, vol. L, San Francisco, California, June 30–July 5, 1996; 145–150.
24. Yoshioka H, Ramallo JC, Spencer BF. Smart base isolation systems employing magnetorheological dampers. *Journal of Engineering Mechanics* (ASCE) 2002; **128**(5):540–551.
25. Park YJ, Wen YK, Ang AHS. Random vibration of hysteritic systems under bi-directional ground motions. *Earthquake Engineering and Structural Dynamics* 1986; **14**(4):543–557.
26. Nagarajaiah S, Narasimhan S. Smart base isolated benchmark building. Part II: Phase. I sample controllers for linear isolation system. *Journal of Structural Control and Health Monitoring* 2006; **13**(2–3):589–604.
27. Yang JN, Li Z, Liu SC. Stable controllers for instantaneous optimal control. *Journal of Engineering Mechanics* (ASCE) 1992; **118**(8):1612–1630.
28. Jabbari F, Schmitendorf WE, Yang JN. $H_\infty$ control for seismic excited buildings with acceleration feedback. *Journal of Engineering Mechanics* (ASCE) 1995; **121**(9):994–1002.
29. Yoshida K, Kang S, Kim T. LQG control and $H_\infty$ control of vibration isolation for MDOF systems. *Proceedings of First World Conference on Structural Control*, vol. TA4, Los Angeles, CA, 1994; 43–52.
30. Nagarajaiah S. Structural vibration damper with continuously variable stiffness. *U.S. Patent 6,098,969*, 2000.
31. MATLAB. *The Math Works, Inc.*, Natick, MA, 2000.
32. Burl BJ. *Linear Optimal Control*. Addison-Wesley/Longman: Reading, MA, New York, 1999.



DOI: 10.1002/eqe

33. Green M, Limebeer DJN. *Linear Robust Control*. Prentice-Hall: Englewood Cliffs, NJ, 1995.
34. Safanov MG, Limebeer DJN. Simplifying the $H_\infty$ theory via loop shifting. *Proceedings of the 27th IEEE Conference on Decision and Control*, Austin, Texas, 1988; 1399–1404.
35. Doyle JC, Glover K, Khargonekar PP, Francis BA. State-space solutions to standard $H_2$ and $H_\infty$ control problems. *IEEE Transactions on Automatic Control* 1989; **34**(8):831–847.
36. Francis BA. *A Course in $H_\infty$ Theory*. Springer: Berlin, 1987.
37. Nagarajaiah S, Reinhorn AM, Constantinou MC. Nonlinear dynamic analysis of 3-d-base-isolated structures. *Journal of Structural Engineering* (ASCE) 1991; **117**(7):2035–2054.
38. Narasimhan S, Nagarajaiah S, Johnson EA, Gavin HP. Smart base isolated benchmark building. Part I: Problem definition. *Journal of Structural Control and Health Monitoring* 2006; **13**(2–3):573–588.



DOI: 10.1002/eqe